Journal of Power Sources 265 (2014) 299–308

Contents lists available at ScienceDirect

Journal of Power Sources

journal homepage: www.elsevier.com/locate/jpowsour

Modified carbon-free silver electrodes for the use as cathodes in lithium–air batteries with an aqueous alkaline electrolyte

Dennis Wittmaier [a,*], Norbert Wagner [a], K. Andreas Friedrich [a,b], Hatem M.A. Amin [c], Helmut Baltruschat [c]

[a] German Aerospace Center (DLR), Institute of Technical Thermodynamics, Pfaffenwaldring 38-40, 70569 Stuttgart, Germany
[b] Institute for Thermodynamics and Thermal Engineering, University of Stuttgart, Germany
[c] Institute of Physical and Theoretical Chemistry, University of Bonn, 53117, Germany

HIGHLIGHTS

- High activity bi-functional catalyst combination for ORR and OER.
- An optimum ratio of high active bi-functional catalysts was found.
- Novel electrodes without carbon to avoid carbon corrosion during OER mode.
- EIS models for ORR and OER describe influence of a growing oxide layers.
- Long-term test exhibited an excellent long-term stability over 200 cycles.

ARTICLE INFO

Article history:
Received 11 March 2014
Received in revised form
14 April 2014
Accepted 29 April 2014
Available online 10 May 2014

Keywords:
Lithium–air battery
Oxygen reduction
Oxygen evolution
Silver electrode
Cobalt oxide electrode
Alkaline electrolyte

ABSTRACT

Gas diffusion electrodes with silver catalysts show a high activity towards oxygen reduction reaction in alkaline media but a rather poor activity towards oxygen evolution reaction. For the use in future lithium–air batteries with an aqueous alkaline electrolyte the activity of such electrodes must be improved significantly. As Co_3O_4 is a promising metal oxide catalyst for oxygen evolution in alkaline media, silver electrodes were modified with Co_3O_4. For comparison silver electrodes were also modified with IrO_2. Due to the poor stability of carbon materials at high anodic potentials these gas diffusion electrodes were prepared without carbon support to improve especially the long-term stability. Gas diffusion electrodes were electrochemically investigated in an electrochemical half-cell arrangement. In addition to cyclic voltammograms electrochemical impedance spectroscopy (EIS) was carried out. SEM and XRD were used for the physical and morphological investigations. Investigations showed that silver electrodes containing 20 wt.% Co_3O_4 exhibited the highest performance and highest long-term stability. For comparison, rotating – ring – disc – electrode experiments have been performed using model electrodes with thin catalyst layers, showing that the amount of hydrogen peroxide evolved is negligible.

© 2014 Elsevier B.V. All rights reserved.

1. Introduction

Today's lithium-ion batteries (LIB) are limited in their capacity due to their active materials used as anode and cathode. The theoretical energy density of LIB's is only 75 to 200 Wh kg^{-1} [1,2]. For future applications in electric vehicles (EV), plug-in hybrid vehicles (PHEV) or in storage devices for renewable energy batteries with far higher energy densities are required to reduce costs, weight and constructed space. The lithium–air battery (LAB) with a metallic lithium anode and an aqueous electrolyte has the theoretical energy density of 12,931 Wh kg^{-1} [3], which is almost as high as the theoretical energy density of gasoline with approximately 13,200 Wh kg^{-1}. Due to limitations in a real cell this theoretical energy density cannot be achieved in practice but still the practical energy density is predicted to increase by factor 5 to 10 compared to today's LIB's. Girishkumar et al. estimate a practical energy density of 1700 Wh kg^{-1} on cell level. This corresponds to 13% of the theoretical value of an aqueous LAB and would be the same as for gasoline [1].

* Corresponding author. Tel.: +49 71168628068; fax: +49 7116862747.
E-mail address: dennis.wittmaier@dlr.de (D. Wittmaier).

http://dx.doi.org/10.1016/j.jpowsour.2014.04.142
0378-7753/© 2014 Elsevier B.V. All rights reserved.

Table 1
Composition of silver- or iridium/cobalt oxide electrodes.

		Ag/wt.%	PTFE/wt.%	Co_3O_4/wt.%	IrO_2/wt.%
Electrode	Pure Ag	90	10	0	0
	5 wt.%	85	10	5	5
	10 wt.%	80	10	10	10
	20 wt.%	70	10	20	20
	30 wt.%	60	10	30	30
	40 wt.%	50	10	40	*x*

Before LAB cells can be used still some limiting factors must be overcome as reported in literature [1,2,4–23]. Main limiting factors are high overpotentials during charge and discharge resulting mostly from deficient catalytic activity of catalysts used on the cathode side of the battery. Catalysts must catalyze the oxygen reduction reaction (ORR) while discharging as well as the oxygen evolution reaction (OER) while charging the battery. Furthermore LAB's suffer from low cyclability and the decomposition of electrode materials. Especially carbon, mostly used in electrodes for metal–air batteries with aqueous alkaline electrolyte, is not stable under oxygen evolution conditions in alkaline media [24–26]. To overcome these limiting factors the main focus of research has to be on sufficient catalysts and a stable electronic conducting support for the cathodes. Co_3O_4 was shown to be a good bi-functional catalyst with high activity towards both reactions [27] and a more inexpensive alternative to noble metal catalysts for future lithium–air batteries with an aqueous alkaline electrolyte. In this paper modified carbon-free bi-functional electrodes with Co_3O_4 and silver were prepared and tested in a half-cell arrangement to improve achieved current densities for ORR and OER compared to pure silver or Co_3O_4 electrodes as well as higher long-term stability compared to common used carbon-based electrodes. The Co_3O_4 content was varied from 5 to 40 wt.% to investigate the improvement of the bi-functional ability. As a benchmark silver electrodes with IrO_2/TiO_2 were also investigated. It was observed that Ag/Co_3O_4 electrodes show a significant improvement compared to pure silver or Co_3O_4 electrodes.

1.1. Lithium–air battery with aqueous alkaline electrolyte

A lithium–air battery with an aqueous electrolyte consists of a lithium metal anode and a porous gas diffusion electrode on the cathode that contains at least one catalyst for the battery reaction. Anode and cathode are separated by a lithium ion conducting separator that protects the lithium metal anode from oxygen and moisture. A protected lithium anode was recently proposed in literature by Visco et al. [28], Zhang and Nobuyuki [29] and Shimonishi et al. [30]. The electrochemistry at the cathode depends on the electrolyte which is used. In this paper cathodes for future LAB's with an aqueous alkaline electrolyte at the cathode were investigated. The fundamental battery reactions are:

$$\text{Cathode: } O_2 + 2H_2O + 4e^- \rightarrow 4OH^- \quad (1)$$

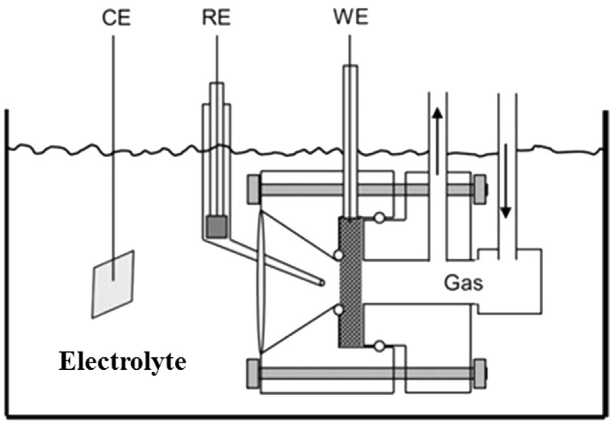

Fig. 1. Half-cell with a three electrode setup in electrolyte tank filled with 1 M LiOH (aq.).

$$\text{Anode: } Li \rightarrow Li^+ + e^- \quad (2)$$

$$\text{Battery reaction: } 4Li + O_2 + 2H_2O \rightarrow 4Li^+ + 4OH^- \quad (3)$$

$$E_0 = 3.45\ V$$

While discharging O_2 is reduced at the cathode according to Equation (1). Simultaneously lithium is oxidized at the anode liberating lithium ions and electrons (Equation (2)). Equation (3) represents the overall battery reaction taking place.

Three catalysts in two combinations were used to prepare electrodes and were tested in a half cell using cyclic voltammetry for analyzing the electrochemical performance of the catalysts. Long-term tests show the stability of the electrodes with these combinations. XRD and SEM were used to investigate the morphology of the catalysts and the electrodes respectively. Electrochemical impedance spectroscopy (EIS) was used to identify loss mechanisms.

2. Experimental

In this chapter the preparation of the electrodes is described as well as the electrochemical and physical characterization methods used in this publication.

2.1. Preparation of electrodes

The Co_3O_4 catalyst powder (99.5%, <50 nm, Sigma Aldrich) was at first hand mixed with Ag (Ag311, Ferro Ag) and PTFE (Hostaflon TF 9207Z, 3 M) as a binder. The IrO_2 catalyst powder (>99%, TiO_2 supported, Umicore) was mixed with Ag and PTFE in the same way. Table 1 shows the individual content of Ag, PTFE and Co_3O_4 or IrO_2 of the prepared electrodes.

After mixing the three materials the compound was again mixed in an electric mill to get a homogeneous mixture. Afterwards the

Table 2
Thickness and loading of silver- or iridium/cobalt oxide electrodes.

		Loading Ag/mg cm^{-2}	Loading Co_3O_4/mg cm^{-2}	Thickness/μm	Electronic resistance/mΩ	Loading Ag/mg cm^{-2}	Loading IrO_2/mg cm^{-2}	Thickness/μm
Electrode	Pure Ag	86.51	0	342	22.25	86.51	0	342
	5 wt.%	76.12	4.48	330	22.25	80.16	4.72	347
	10 wt.%	71.12	8.89	343	28.58	73.32	9.14	328
	20 wt.%	64.73	18.49	367	29.27	68.15	19.47	377
	30 wt.%	56.11	28.05	362	572	55.76	27.88	378
	40 wt.%	46.33	37.06	397	*x*	*x*	*x*	*x*

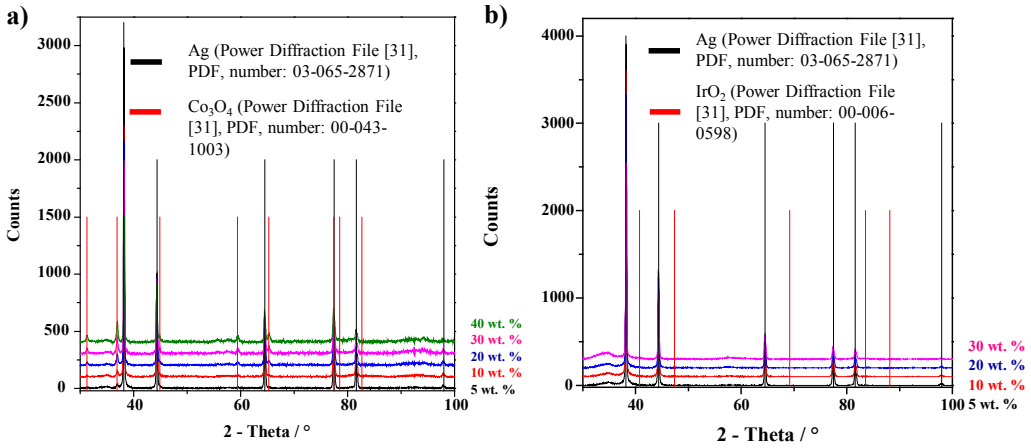

Fig. 2. XRD patterns of Ag electrodes with various (a) Co_3O_4 and (b) IrO_2 content [31].

mixed powder was filled in a flexible forming frame and covered with a stainless steel net which is used as a current collector and mechanical strength enhancer at the same time. This setup was put between two metal plates and then pressed in a hydraulic press resulting in a gas diffusion electrode. After pressing the electrodes were sintered in an oven for 1 h at 340 °C in ambient air to fix the catalyst layer. The average thickness of the electrodes was 360 μm. The exact thickness and loading of each electrode can be found in Table 2.

2.2. Electrochemical characterization

The electrochemical tests were carried out in half-cell with a three electrode setup (Fig. 1). In this setup the gas diffusion electrode is the working electrode whereas a platinum-electrode is used as counter electrode. The electrochemical potential is measured between the working electrode and a reversible hydrogen electrode RHE (HydroFlex, Gaskatel).

The active area of the half-cell is 1 cm^2. To reduce the contact resistance between the current collector of the half-cell and the electrode, the electrode is additionally stacked with a Sigracet® GDL 35DC towards the gas inlet. For the measurements the half-cell was put in an electrolyte tank filled with 1000 ml of 1 M LiOH (aq.) and maintained at 25 °C. The testing gas was purified oxygen (O_2). Cyclic voltammograms (CV), potentiostatic curves (PC) and electrochemical impedance spectra were carried out with a Zahner IM6 Electrochemical Workstation. Electrodes were cycled between 0.3 and 1.8 V versus RHE with a scan rate of 1 mV s^{-1}. Pre-tests have shown that after 20 cycles there is a stable behavior, so before carrying out the impedance measurements and PC every electrode was cycled 20 times. For PC's the electrodes were held for 15 min at 0.3 and 1.8 V vs. RHE. Potentiostatic EIS was carried out at open cell voltage (OCV) and at OCV ± 100 mV, ±300 mV, ±500 mV, ±700 mV. The frequency range for EIS was 100 mHz to 100 kHz with an amplitude of 5 mV. For the long-term tests the electrodes were cycled for 200 cycles with the same scan rate of 1 mV s^{-1} after the standard investigations done on all electrodes.

Rotating ring-disc electrode (RRDE) measurements were conducted in a three-compartment glass cell using a bipotentiostat and RRDE assembly from Pine Research Instrumentation, USA. A glassy carbon (GC) electrode modified by the catalyst served as the working electrode. The reference electrode was a reversible hydrogen electrode (RHE) in the same electrolyte. As a counter electrode, Pt sheet was used. The catalyst powder was ultrasonically dispersed in ethylene glycol for at least 30 min. Differently from the gas diffusion electrodes as described above, no PTFE was added. An appropriate amount of the suspension was pipetted onto a pre-polished GC support (5 mm diameter) leading to 1 mg cm^{-2}_{disc} catalyst loading. 20 μl of diluted Nafion® solution was placed on top of the dried catalyst to attach it to the GC. The prepared electrode was then installed in the tip of the rotor. ORR measurements were done in O_2-saturated solution at room temperature (25° ± 1).

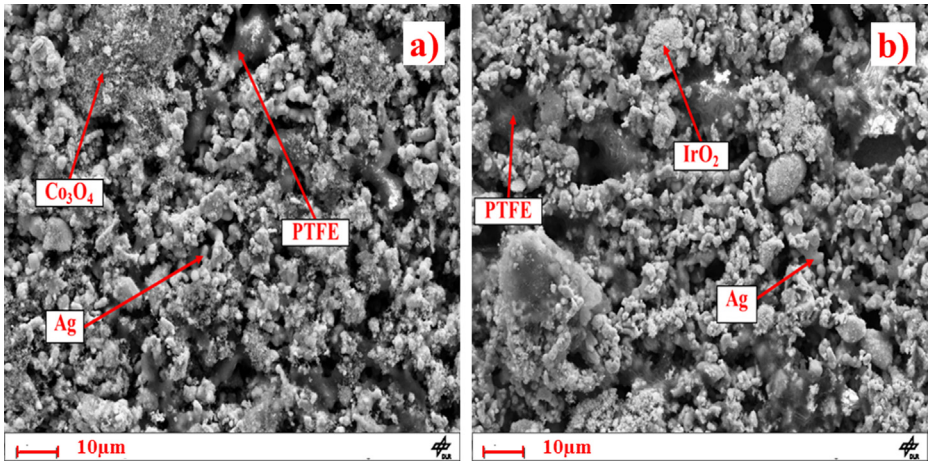

Fig. 3. SEM images of Ag electrodes mixed with (a) 20 wt.% Co_3O_4 and (b) 20 wt.% IrO_2.

2.3. XRD, SEM and electronic conductivity

Electrodes and catalysts were examined with XRD, SEM and EDX. X-ray diffractograms were measured with a X-ray diffractometer, D8 Discover GADDS with a VÅNTEC-2000 area detector. Exposures were carried out in reflexion mode with a tuned monochromatic and parallel X-ray beam (Cu-K_α), with a tube collimator aperture of 1 mm. The accelerating voltage was 45 kV and the tube current was 0.650 mA. Each diffraction pattern was measured in four frames with a step size of 23° (start $\Theta_1 = \Theta_2 = 12°$). The exposure time was 180 s for each frame. For morphology the electrodes were examined with a Zeiss ULTRA plus SEM with Charge Compensation. In this work secondary electron images (SE) as well as back-scattered electron images (BSE) are shown. In addition to XRD and SEM electronic conductivity measurements of the electrodes were carried out. Therefore the electrodes were stacked with a Sigracet® GDL 35DC as in the half cell and put between two gold coated testing electrodes and load of 3 kg was applied via a pressure unit. The testing electrodes were connected to the Zahner IM6 and EIS spectra were carried out to observe the electronic resistance.

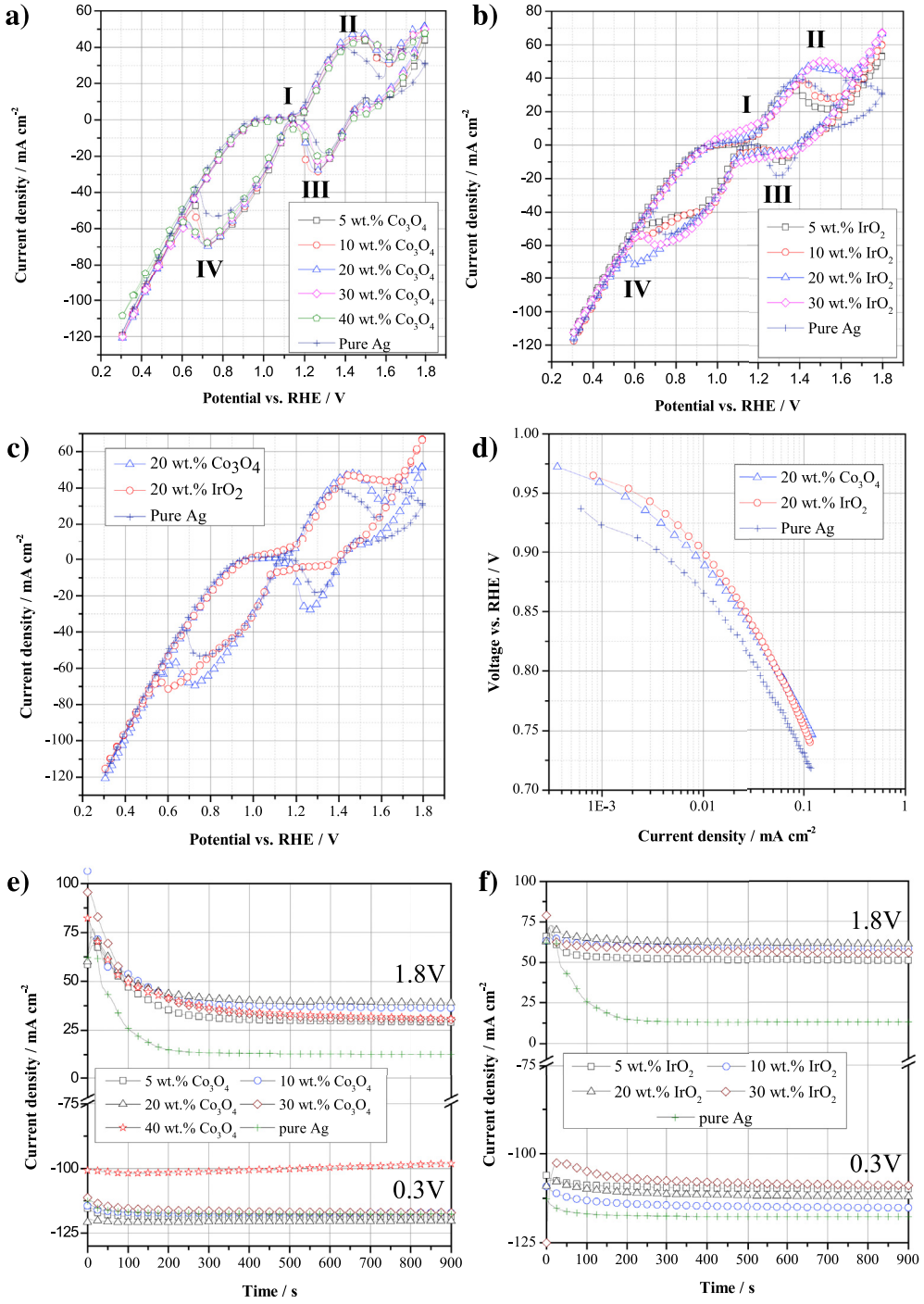

Fig. 4. Results of CV's for (a) Co_3O_4/Ag-, (b) Ag/IrO_2-electrodes, the (c) comparison of the best combinations, (d) the Tafel plots of the best combinations and (e) + (f) the potentiostatic curves in 1 M LiOH (aq.) at 25 °C.

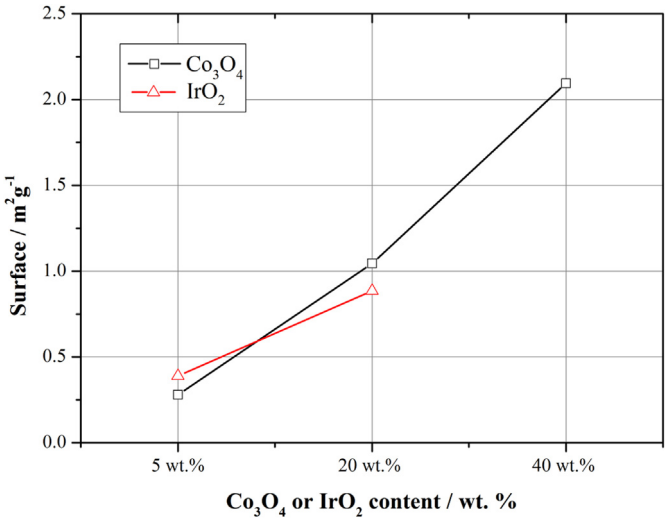

Fig. 5. Increasing surface of Ag electrodes with increasing Co_3O_4 or IrO_2 content.

3. Results and discussion

The electrodes with varying Co_3O_4 and IrO_2 content were investigated by XRD. Fig. 2a and b shows the XRD pattern of Ag/Co_3O_4 and Ag/IrO_2 electrodes respectively.

Co_3O_4 electrodes agreed perfectly with XRD standard data. Some Co_3O_4 peaks start to appear at 10 wt.% and constantly grow until 40 wt.% electrodes. Ag phase shows very good intensity. XRD spectra of the different IrO_2 electrodes show also an Ag phase with a very high intensity while the IrO_2 shows very low intensity (around 20 counts) due the very small particle size and high amorphous structure and is therefore not visible in Fig. 2b.

Fig. 3a and b shows silver electrodes mixed with Co_3O_4 and IrO_2. It can be seen that the global electrode structure is similar. Both, Co_3O_4 and IrO_2 particles form agglomerates and partly cover the bigger sized Ag particles. The used components were identified by EDX.

3.1. Cyclic voltammetry

As described in Section 2.1 the content of Co_3O_4 and IrO_2 was varied in the steps as shown in Table 1. The so prepared electrodes were measured in a half-cell as described in Section 2.2. The resulting CV's (not iR-corrected) are shown in Fig. 4a and b. For comparison the CV's of pure silver electrodes are also shown in Fig. 4a–c.

As one can see in Fig. 4a the addition of Co_3O_4 to the pure silver electrode enhances current density for the OER significantly. With an increasing Co_3O_4 content the current densities also increase constantly and reach a maximum at a content of 20 wt.% Co_3O_4 and 70 wt.% Ag respectively. The CV's for Ag/Co_3O_4 as well as for Ag/IrO_2 show typical redox-peaks of silver with the anodic peaks I and II and the cathodic peaks III and IV. Peak I can be divided in three sub-peaks which are associated with the formation of AgOH and soluble Ag(I) species as well as an inner hydrous Ag(I) and a compact outer Ag(I) oxide layer. In contradiction with Tudela [32], we observed the electroformation Ag(I) → Ag(II) already reported in Refs. [33–36]. This oxidation corresponds to peak II in Fig. 4a and b. Cathodic peaks III and IV are corresponding to the reduction of Ag(II) to Ag(I) and Ag(I) to Ag. The current density for the ORR is mainly dominated by the activity of silver and stays nearly constant for all electrodes. The only exception is the 40 wt.% Co_3O_4 electrode which a lower current density for the ORR as well as for the OER. The lower current density is mainly due to the increasing electronic resistance with an increasing Co_3O_4 content as BET surface is increasing with the increasing Co_3O_4 content of the electrode (Fig. 5). So performance is not directly increasing with the BET surface. Electronic resistance seems to have a higher influence after reaching 20 wt.% Co_3O_4. Current density already starts to lower at a Co_3O_4 content of 30 wt.% and increases rapidly afterwards. Table 2 shows the electronic resistance of the tested electrodes and the rapidly increasing resistance between 30 and 40 wt.% Co_3O_4.

For the IrO_2 electrodes one can also see an improvement of the current density for the OER but not for ORR (Fig. 4b). In this combination of catalysts the activity of silver also dominates the ORR. As for Co_3O_4 the current densities for the OER increase with an increasing content of IrO_2 up to a certain content of IrO_2. OER current density for 30 wt.% stays the same as for 20 wt.% and there is no loss of current density for ORR. In contrast to Ag/Co_3O_4 electrodes the electronic resistance does not increase at 30 wt.% IrO_2. Due to the high price of IrO_2 and no further increased current density 20 wt.% IrO_2 seems to be an optimum composition.

Fig. 4c shows the comparison of the 20 wt.% CV's with Co_3O_4 and IrO_2 electrodes compared to the pure silver. IrO_2 shows the highest OER current density, even better than Co_3O_4. The Co_3O_4 electrodes on the other hand show a higher ORR current density than both other electrode types. The combination of Co_3O_4 and silver seem to improve ORR current density even though pure Co_3O_4 does exhibit a lower ORR current density than pure silver.

Fig. 4d shows the cathodic Tafel plots of the 20 wt.% Co_3O_4 or IrO_2 containing electrodes as well as the one of the pure silver electrode. One can see all electrodes show a different polarization behavior what is due to the use of the different catalysts exhibiting different electrocatalytic behavior. The pure silver electrode exhibits the lowest current density of all electrodes while the two catalyzed electrodes show improved performance. The Tafel plot is an iR-corrected illustration and therefore it can be seen that not only Co_3O_4 catalyzed electrodes show higher ORR current density than pure silver electrodes but also IrO_2 catalyzed electrodes. Even though IrO_2 electrodes show higher current densities than pure silver electrodes Co_3O_4 electrodes exceed these, exhibiting the highest ORR current densities at the lowest recorded potential starting from OCV. At lower overpotentials there is an initial

Table 3
Maximum and sum of current densities from 20 wt.% Co_3O_4 and IrO_2 electrodes at 300 mV and 1800 mV in comparison with pure Ag electrode in 1 M LiOH (aq.), feed gas O_2, 25 °C, ambient pressure and a scan rate of 1 mV s^{-1}.

		Cathodic current density Co_3O_4/mA cm^{-2}	Anodic current density Co_3O_4/mA cm^{-2}	Sum current density Co_3O_4/mA cm^{-2}	Cathodic current density IrO_2/mA cm^{-2}	Anodic current density IrO_2/mA cm^{-2}	Sum current density IrO_2/mA cm^{-2}
Electrode	Pure Ag	118	30.9	148.9	118	30.9	148.9
	5 wt.%	119.5	43.9	163.4	112	52.5	164.5
	10 wt.%	119.5	48.55	168.05	117.5	59.85	177.35
	20 wt.%	120.5	51.43	171.93	116	66.6	182.6
	30 wt.%	120.15	50.03	170.18	112.25	67	179.25
	40 wt.%	108.65	47.5	156.15	*x*	*x*	*x*

advantage of the IrO_2 catalyzed electrodes over the Co_3O_4 catalyzed. This is changing from approximately 825 mV vs. RHE.

Table 3 shows the maximum and sum of the cathodic and anodic current densities in the potential range of 0.3–1.8 V of both combinations compared to pure silver electrodes. At the optimum composition of 20 wt.% for either Co_3O_4 or IrO_2 the absolute difference between these two combinations is only 10.67 mA. Considering the high price for IrO_2 Co_3O_4 is a more reasonable catalyst for the use in bi-functional cathodes in future LAB's.

For the future use in an LAB with an aqueous alkaline electrolyte not only cycling performance and maximum current density are important. Electrodes must exhibit stable current densities while charging- and discharging-process. Therefore potentiostatic curves were recorded to obtain the current over time behavior of the electrodes.

Fig. 4e illustrates the potentiostatic curves for the Ag/Co_3O_4 electrodes. After an initial drop in current density (OER, 1.8 V) due to a growing (silver-) oxide layer on the surface of the electrodes the current densities remain nearly stable after 200 s. The 30 wt.% electrodes have the highest current density drop for OER and exhibit nearly the same value as the 5 and 40 wt.% electrodes. In case of the 30 and 40 wt.% electrode this is due to the higher electronic resistance, in case of the 5 wt.% to the low Co_3O_4 content. As already seen in the CV's the 20 wt.% electrodes exhibit the highest current density for OER as well as for ORR. In ORR all electrodes exhibit a stable behavior without an initial current density drop. With exception of the 40 wt.% electrode all electrodes are in the same current density range but for 30 wt.% the current densities starts to be lower than for pure silver electrodes. The combinations of Ag with 5, 10, and 20 wt.% Co_3O_4 show a higher current density than pure silver electrodes.

In Fig. 4f the same potentiostatic curves for the Ag/IrO_2 electrodes can be seen. As expected from the CV's these electrodes also exhibit a higher current densities in OER than Ag/Co_3O_4 electrodes and they remain stable as well. In comparison to the Ag/Co_3O_4 electrodes there is only a slight initial current drop for OER, what indicates a higher initial activity for OER of these electrodes due to the use of IrO_2. 20 wt.% electrodes also exhibit the highest current densities for OER. Higher contents increase the electronic conductivity slightly and therefore lower the achieved current densities as it can be seen for 30 wt.%. The lowest current density of 5 wt.% is due to the low IrO_2 content. Compared to Co_3O_4 electrodes the ORR current density is slightly lower and there is a higher spread between the current densities of the electrodes with varying IrO_2 content. Pure silver electrodes exceed the ORR current densities of the IrO_2-modified electrodes. The use of IrO_2 does not increase the achieved current density for ORR as seen for Co_3O_4.

3.2. RRDE measurements

Cyclic voltammetry of a thin layer of the catalysts on a glassy carbon electrode is shown in Fig. 6a. In the anodic scan, a diffusion-limited current is observed, in the potential range of kinetic control (between 0.6 and 0.9 V) the 10 wt.% Co_3O_4 catalyst is more active than pure Ag (curve shifted by about 50 mV in anodic direction), whereas the 20 wt.% Co_3O_4 catalyst is somewhat less active. At potentials close to oxygen evolution, the currents in the anodic scan are dominated by the oxidation of Ag to the Ag(I) and higher oxidation states. In the cathodic scan, the current is due to oxygen evolution, which is fastest on the 20 wt.% Co_3O_4 catalyst. For the Co_3O_4 modified catalysts, currents in cathodic direction are identical to steady state currents obtained after potential stops for 3 min both during the anodic and cathodic scan. For pure Ag, steady state currents decrease below the current of the cathodic scan. Similar results were obtained in 1 M LiOH.

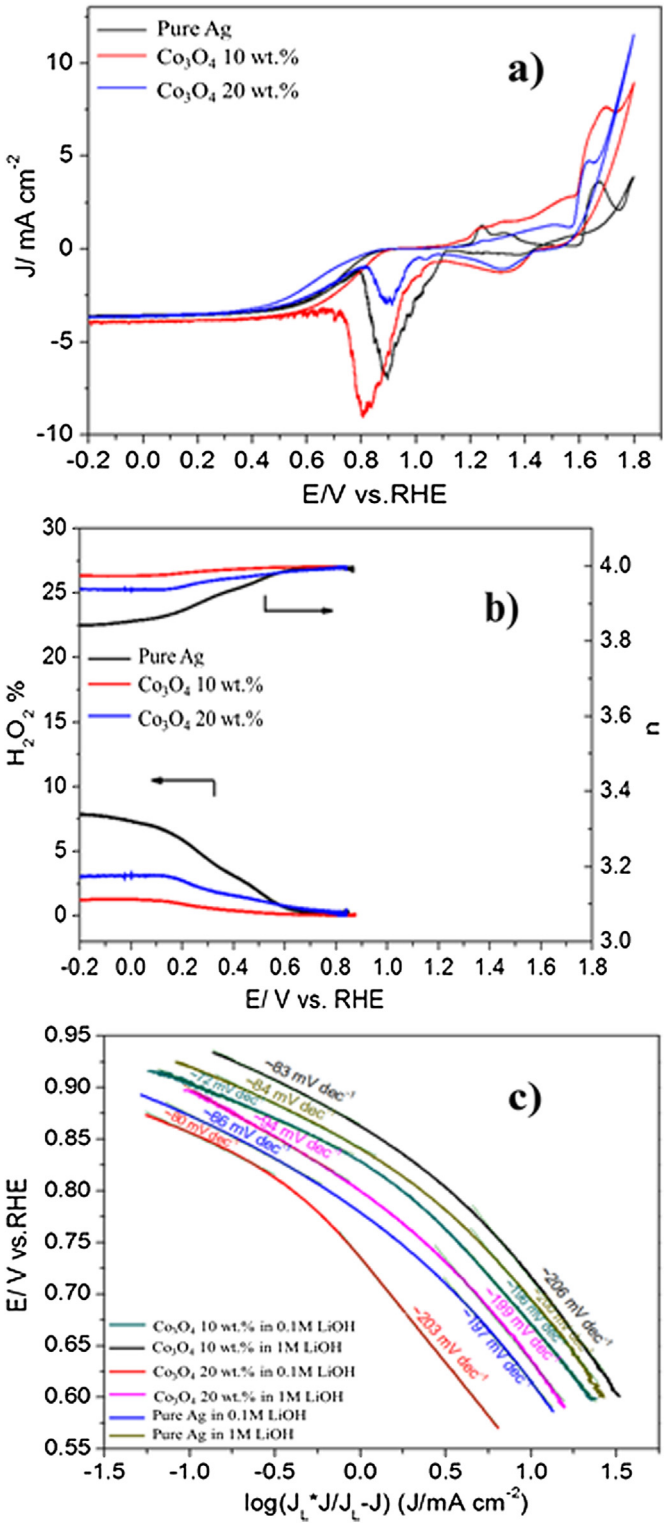

Fig. 6. RRDE polarization curves (a) of catalysts as indicated in O_2-saturated 0.1 M LiOH solution with scan rate of 5 mV s^{-1} and rotation rate of 960 rpm (1 mg cm^{-2} loading), (b) percentage of peroxide (left axis) and electron transfer number *n* (right axis) at various potentials obtained from the corresponding data in (a) and (c) the Tafel plots obtained from the corresponding CV's with 5 mV s^{-1} and 960 rpm.

Obviously, a small amount of Co_3O_4 enhances the catalytic activity of the Ag. A similar effect was observed for carbon supported Ag–Co catalysts before for oxygen reduction [37,38] and can be ascribed to altered electronic properties, a special catalytic activity

of the triple phase boundary between the solution and the two catalysts or a bifunctional mechanism of the two catalysts involving surface diffusion of an intermediate. An influence of the Co_3O_4 on the surface roughness and prevention of coagulation of the Ag particles also has to be considered.

The amount of hydrogen peroxide formed (as calculated from the ring currents) is almost negligible and reaches less than 3% over the entire range for the mixed catalysts and less than 8% for Ag. Accordingly, the number of electrons transferred is always between 3.8 and 4, as shown in Fig. 6b. Therefore, these catalysts obey the 4-electron pathway for ORR. For comparison, for carbon supported Ag and Ag–Co catalysts between 2.7 and 3 were reported [37].

Mass-transport corrected Tafel plots (log J_k vs. E) are shown in Fig. 6c. The kinetic current (J_k) was expressed as $J_L \times J/J_L - J$, where J_L is the diffusion limited current density and J is the measured current density. The kinetic current is higher for the 10% catalyst compared to pure Ag catalyst towards ORR both in 0.1 M and 1 M LiOH, but lower at the catalyst with 20 wt.% Co_3O_4. At low overpotentials, Tafel slopes of about 80 mV dec^{-1} were obtained for these catalysts. This value is close to the 60 mV dec^{-1} which suggests a dissociative

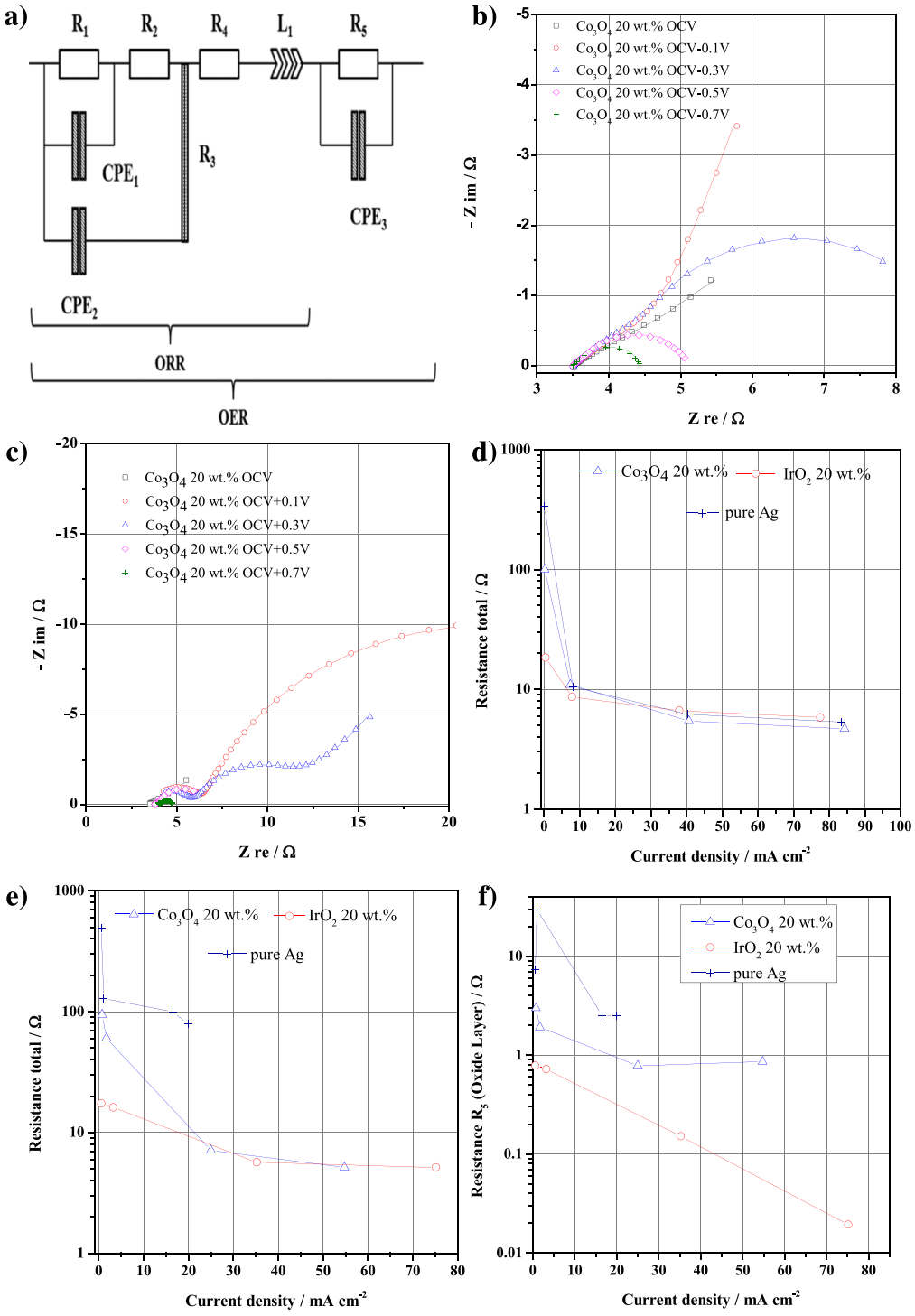

Fig. 7. Fitting results of EIS with (a) two different models for the 20 wt.% Co_3O_4 electrodes in (b) ORR and (c) OER as well as R_{total} for (d) ORR, (e) OER and the (f) resistance R_5.

mechanism, in which the rate determining step involves dissociative adsorption of one molecule of oxygen through a 2-electron transfer process [39,40]. A higher overpotentials, a slope of about 200 mV dec^{-1} was obtained for all of the catalysts.

3.3. Electrochemical impedance spectroscopy (EIS)

To gain additional information about the electrodes EIS characteristics have been evaluated. For the fitting of the impedance spectra two different models were used. For ORR the left part of Fig. 7a was used as model. R_1 and the constant phase element CPE_1 represent the adsorption of oxygen on the catalytic active surface of the electrode. R_2 is related to the charge transfer process at the catalyst surface while CPE_2 represents the double layer capacitance. As a gas diffusion electrode has a porous structure the model should consider this structure due to the influence of the structure on current density. In this model this has been done with R_3. R_3 represents the electrolyte resistance inside a porous electrode on basis of homogenous pore system impedance simulation by Göhr [41]. Resistance R_4 includes the ohmic resistance of the electrolyte and the contacts. L_1 represents an inductor considering inductances of for example cables or current collectors.

In addition to the ORR model in the left part of Fig. 7a for OER the ORR model was used with the extension in the right part of Fig. 7a. The OER model is similar to the ORR model but it has been adapted with another parallel R/CPE element which is related to a growing oxide layer on the surface of the electrode during oxygen evolution operation.

Fig. 7b and c shows fitting results of Co_3O_4 20 wt.% electrodes as solid line. The fitting parameter values of the other electrodes can be seen in Table 4.

Simulation results show very good agreement with the measured characteristics for both models. Fig. 7d and e shows the total resistances of the tested electrodes over their corresponding current density. One can see that the characteristics correspond to the measured CV's for the electrodes and total losses through resistances are decreasing with an increasing current density. The total resistances are mainly determined by the resistances R_1, R_2, R_3 and in case of OER also by R_5. As there is no significant difference for ORR current densities and therefore in the losses, OER parameters are more of interest. The corresponding resistances of R_5 (Fig. 7f) fit to the current densities from the CV's. Pure silver which is

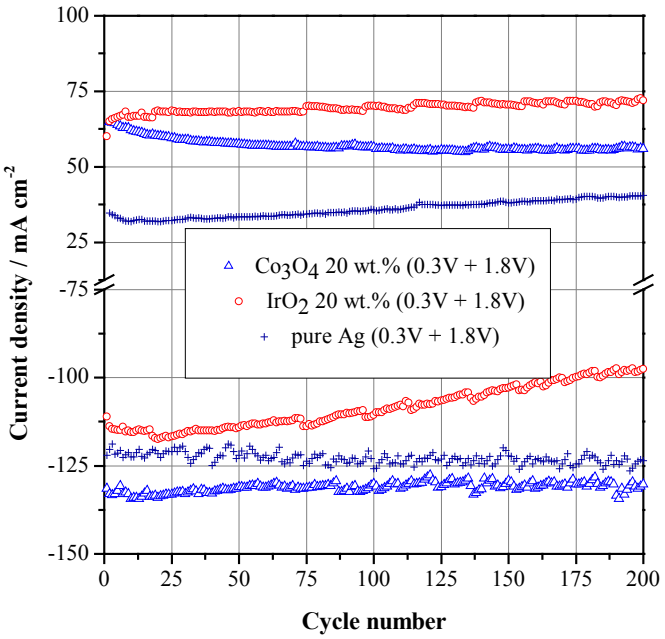

Fig. 8. Current densities at 0.3 V and 1.8 V vs. RHE of pure silver, 20 wt.% Co_3O_4 and 20 wt.% IrO_2 electrodes over 200 cycles at 25 °C in 1 M LiOH (aq.) with feed gas O_2.

Table 4
Fitting parameters of Ag, Ag/Co_3O_4 and Ag/IrO_2 – electrodes at different cathodic and anodic potentials. Spectra recorded at 25 °C in 1 M LiOH (aq.) with feed gas O_2 in the frequency range from 100 mHz to 100 kHz.

Sample	R1/Ω	CPE 1/F	R2/Ω	CPE 2/F	R3a/Ω	R3b/Ω	R4/Ω	L1/H	R5/Ω	CPE 3/F
Pure Ag OCV	5.74E+00	4.84E-02	1.78	1.91E-02	1.75	1.48E-01	3.36	1.91E-07	*x*	*x*
Pure Ag OCV − 0.1 V	3.27E+02	1.56E-02	2.20	1.62E-02	2.33	2.70E-01	3.26	1.83E-07	*x*	*x*
Pure Ag OCV − 0.3 V	3.43E+00	2.64E-02	1.65	1.28E-02	1.84	1.25E-01	3.39	1.71E-07	*x*	*x*
Pure Ag OCV − 0.5 V	5.69E-01	2.73E-02	0.78	8.57E-03	1.36	1.63E-01	3.35	1.75E-07	*x*	*x*
Pure Ag OCV − 0.7 V	3.16E-01	2.47E-02	0.47	6.48E-03	1.02	1.82E-01	3.33	1.74E-07	*x*	*x*
Pure Ag OCV	4.54E+00	7.44E-01	0.10	4.74E-06	1.79	5.06E-02	3.04	2.81E-07	4.30E+00	1.49E-03
Pure Ag OCV + 0.1 V	3.35E+01	5.25E-03	1.48	1.12E-04	60.72	2.74E-02	3.32	2.87E-07	2.95E+01	2.08E-04
Pure Ag OCV + 0.3 V	4.53E+02	9.79E-04	26.69	5.08E-04	5.80	1.66E-02	3.71	8.51E-09	7.34E+00	7.62E-06
Pure Ag OCV + 0.5 V	4.54E-01	2.04E-01	16.70	1.30E-05	77.63	3.20E-02	2.51	2.75E-07	2.53E+00	2.63E-04
Pure Ag OCV + 0.7 V	3.85E+01	1.47E-01	0.02	1.35E-05	35.03	3.78E-02	2.84	2.15E-07	2.51	6.30E-04
Co_3O_4 20 wt.% OCV	1.38E+01	5.67E-03	9.57	4.92E-02	4.30	1.04E-02	3.48	9.61E-08	*x*	*x*
Co_3O_4 20 wt.% OCV − 0.1 V	6.80E+01	4.77E-03	25.04	3.71E-02	3.25	1.26E-02	3.48	8.76E-08	*x*	*x*
Co_3O_4 20 wt.% OCV − 0.3 V	3.32E+00	4.91E-03	1.15	2.44E-02	2.95	2.04E-02	3.47	1.06E-07	*x*	*x*
Co_3O_4 20 wt.% OCV − 0.5 V	1.11E+00	2.65E-04	0.45	2.51E-03	0.41	2.11E-02	3.44	1.02E-07	*x*	*x*
Co_3O_4 20 wt.% OCV − 0.7 V	6.44E-01	3.12E-04	0.27	2.21E-03	0.29	2.24E-02	3.44	8.85E-08	*x*	*x*
Co_3O_4 20 wt.% OCV	9.14E+00	8.77E-03	25.57	5.71E-02	4.80	1.19E-02	3.17	9.25E-08	3.04E-01	1.63E-07
Co_3O_4 20 wt.% OCV + 0.1 V	6.20E+01	1.46E-03	25.99	2.80E-04	0.43	2.35E-02	3.28	2.73E-07	3.00	3.84E-07
Co_3O_4 20 wt.% OCV + 0.3 V	4.66E+01	7.76E-03	6.46	7.48E-04	1.74	2.51E-02	3.55	7.95E-08	1.92	3.66E-06
Co_3O_4 20 wt.% OCV + 0.5 V	2.12E-02	7.01E-03	2.76	1.84E-02	0.51	6.91E-02	2.96	2.38E-08	0.79	2.10E-07
Co_3O_4 20 wt.% OCV + 0.7 V	4.82E-03	4.96E-03	0.64	1.12E-02	0.49	7.63E-02	3.09	1.36E-08	0.86	4.17E-07
IrO_2 20 wt.% OCV	14.38	3.420E-01	3.87E+00	7.40E-03	0.28	9.54E-02	3.67	1.56E-07	*x*	*x*
IrO_2 20 wt.% OCV − 0.1 V	10.12	2.100E-01	4.16E+00	5.39E-03	0.30	1.22E-01	3.65	1.55E-07	*x*	*x*
IrO_2 20 wt.% OCV − 0.3 V	2.25	1.390E-01	2.24E+00	5.11E-03	0.32	2.10E-01	3.61	1.71E-07	*x*	*x*
IrO_2 20 wt.% OCV − 0.5 V	1.51	1.160E-01	2.17E-04	1.46E-02	1.40	6.79E-03	3.73	1.16E-07	*x*	*x*
IrO_2 20 wt.% OCV − 0.7 V	0.87	1.050E-01	1.73E-04	1.64E-02	1.23	7.25E-03	3.72	1.29E-07	*x*	*x*
IrO_2 20 wt.% OCV	1.09E+01	4.13E-01	2.51	1.33E-02	0.42	4.26E-02	3.37	1.67E-07	3.29E-01	1.50E-08
IrO_2 20 wt.% OCV + 0.1 V	6.71E+00	1.01E-01	4.27	1.46E-02	1.68	2.03E-02	3.90	1.17E-07	0.79	1.76E-04
IrO_2 20 wt.% OCV + 0.3 V	5.92E+00	1.17E-01	3.84	1.60E-02	1.74	2.00E-02	3.92	8.10E-08	0.72	2.18E-04
IrO_2 20 wt.% OCV + 0.5 V	1.16E-01	8.06E+00	0.58	8.38E-02	0.95	2.92E-02	3.85	1.06E-07	0.15	1.23E+00
IrO_2 20 wt.% OCV + 0.7 V	6.69E-02	1.84E+01	0.34	4.56E-02	0.80	3.08E-02	3.90	1.00E-07	0.02	1.87E+00

exhibiting the lowest current density is also showing the highest resistances and in difference to the Co_3O_4 and IrO_2 no constant decreasing characteristic with an increasing current density. This is mainly due to the reactions taking place on silver during oxygen evolution, as there is the oxidation of silver to Ag_2O and higher oxidation states as well as the oxygen evolution reaction at the same time. IrO_2 shows the lowest overall resistances what is corresponding to CV results. Especially R_5 which represents the forming oxide layer shows that IrO_2 electrodes have the lowest losses and therefore the highest current densities.

3.4. Long-term tests

To investigate the cycling stability of the electrodes long-term tests were carried out. Therefore the electrodes were cycled 200 times under the same conditions as for the CV's before. Fig. 8 shows the current density trends of the tested electrodes at the maximum potentials for ORR and OER which were 0.3 V and 1.8 V vs. RHE respectively.

As one can see all electrodes seem to be relatively stable over 200 cycles. The pure silver electrode remains stable for ORR current density, while the OER current density increases slightly during cycling. The Ag/Co_3O_4 electrodes with 20 wt.% cobalt oxide show higher current densities in ORR as well as OER compared to pure Ag as expected. During the first 50 cycles these electrodes show a slight degradation in OER performance but remain stable afterwards. Considering the characteristics of the pure silver electrode and the SEM images (Fig. 9A–C and a–c) this degradation might be due to a little loss of active material (cobalt oxide) on the surface which dominates the OER. SEM images show a rougher surface which indicates cobalt oxide particles might get lost due an increasing gas pressure in the pores of the electrode during oxygen evolution. Due to this gas pressure the small cobalt oxide particles might lose adhesion. As OER current density of pure silver

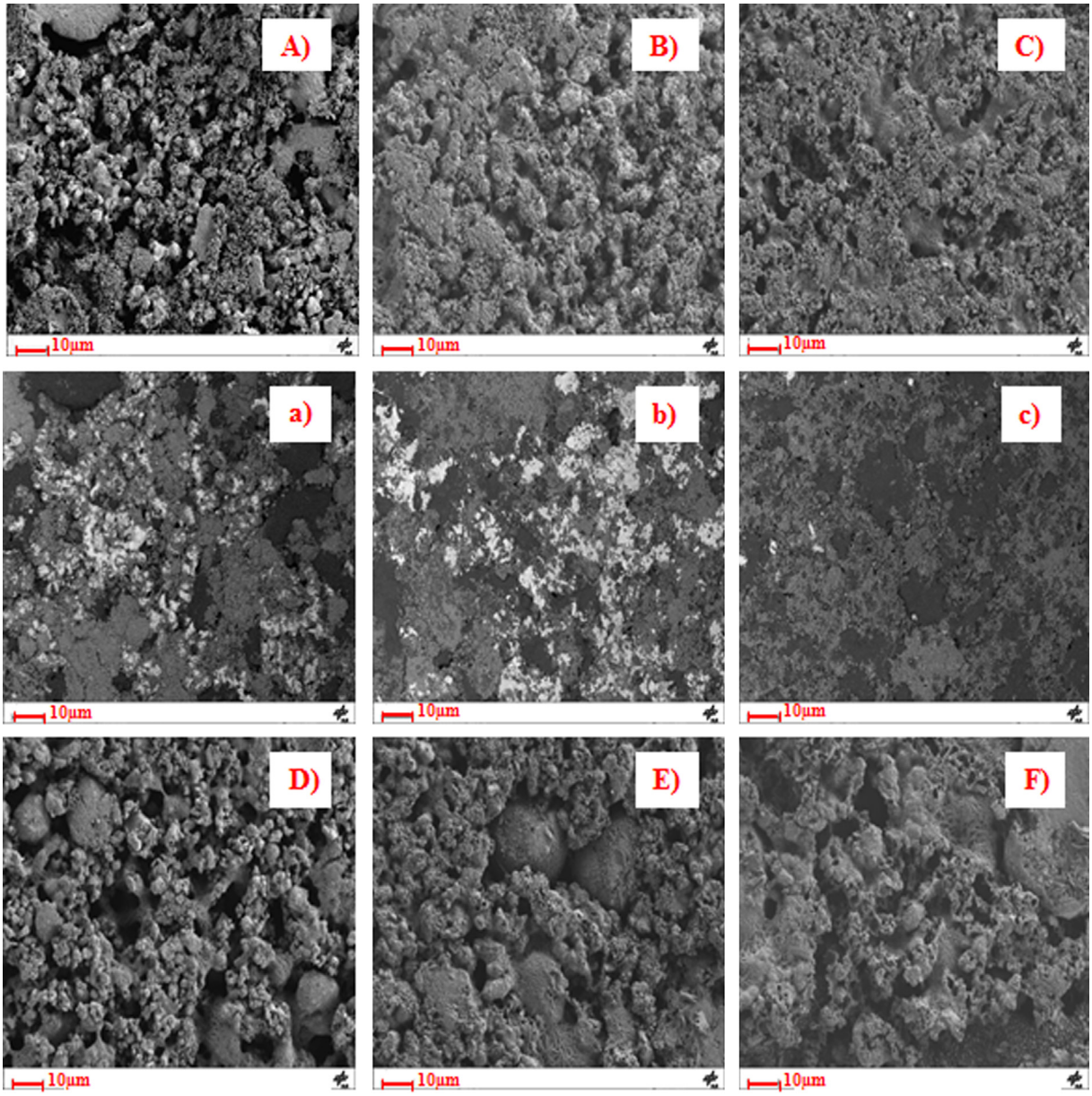

Fig. 9. SE (A–C) and BSE (a–c) images of 20 wt.% Co_3O_4 modified Ag electrodes (Ag corresponds to white areas in BSE images) and SE images (D–F) of 20 wt.% modified IrO_2 electrodes after 0, 20 and 200 cycles.

electrodes increases over cycling due to an increasing surface of these electrodes the loss of active material in the Ag/Co_3O_4 combination is a possible reason. SEM images of an electrode after 20 cycles (Fig. 9B and b) show that cobalt oxide started to cover the silver particles throughout cycling which might be the reason for the increasing current density from the first to the 20th cycle caused by a more homogenous distribution of the active materials. The covering might decrease the contact resistance between agglomerates of cobalt oxide and silver as well as increases the active surface of initially agglomerated cobalt particles. This coverage continues in the long-term tests after the initial 20 cycles. Fig. 9C and c shows the cycled electrode after 200 cycles long-term test.

Iridium oxide electrodes show a stable behavior for OER but degrade during cycling for ORR. SEM images (Fig. 9D–F) look the same as for Co_3O_4 electrodes. The surface is getting rougher over cycling. In difference to the Ag/Co_3O_4 electrodes Ag/IrO_2 electrodes show not even a slight degradation for OER which indicates that there is no loss in active iridium oxide area. Since silver is stable over cycling the loss for ORR has another reason. All tested IrO_2 electrodes exhibited cracks in the active area of the electrode after cycling.

This might be due to the good activity of IrO_2 for the OER. High gas pressure in the pores during OER leads to mechanical stress in the catalyst layer. These cracks cause a flooding of the electrode resulting in a loss of ORR performance [4] due to the slow solubility of oxygen in the aqueous electrolyte. Furthermore the ohmic resistance of the electrode might increase due to the decreasing electronic conducting paths in the electrode. The stable OER behavior indicates that the flooding is main reason for the decreasing current density because OER current density was not influenced by a flooded electrode.

4. Conclusions

Carbon-free pure silver electrodes for aqueous alkaline lithium–air batteries with a high activity in ORR were modified with Co_3O_4 nano-particles to improve current density for the OER. In addition pure silver electrodes were modified with highly active IrO_2 as a benchmark. CV's were carried out for electrodes with varying Co_3O_4 and IrO_2 content to obtain the optimum ratio for the electrode performance between silver and Co_3O_4 or IrO_2 respectively. For both, Co_3O_4 and IrO_2, 20 wt.% turned out to be the optimum. The use of Co_3O_4 and IrO_2 improved OER current density of the electrodes significantly. ORR current density was also influenced by Co_3O_4 and IrO_2. Electrodes with Co_3O_4 and IrO_2 showed a slight improvement in ORR performance in comparison to pure silver electrodes. Potentiostatic curves at 0.3 V and 1.8 V proofed the stability of the electrodes for charge- and discharge-mode. RRDE experiments using thin catalyst layers as model electrodes confirm the results. The somewhat different optimum composition for oxygen reduction might be due the absence of nafion or slight difference in the preparation. Long-term stability was investigated with a 200 full-cycle test in a half-cell. Pure silver as well as Ag/Co_3O_4 electrodes exhibited very stable behavior; especially Ag/Co_3O_4 electrodes exhibited high current densities over 200 cycles with only a slight degradation due to the loss of active material on the surface. IrO_2 electrodes show degradation for ORR due to cracks in the catalysts layer resulting in a flooded gas diffusion electrode. Electrochemical impedance spectra identified the ohmic resistance increase through a growing oxide layer as the main reason for the performance advantage of Ag/IrO_2 electrodes over Ag/Co_3O_4 electrodes. Considering the high price of IrO_2 and the degradation for ORR Ag/Co_3O_4 electrodes are a more reasonable and high energy density alternative for Li–air batteries.

Acknowledgment

Thank you to the Federal Ministry of Education and Research for funding this work. This work is part of the "LuftLi – Strom aus Luft und Lithium" project (FKZ:03X4624C and FKZ:03X4624A). H.M.A. Amin thanks DAAD and MoHESR for a scholarship.

Appendix A. Supplementary data

Supplementary data related to this article can be found at http://dx.doi.org/10.1016/j.jpowsour.2014.04.142.

References

[1] G. Girishkumar, B. McCloskey, A.C. Luntz, S. Swanson, W. Wilcke, J. Phys. Chem. Lett. 1 (2010) 2193.
[2] R. Padbury, X. Zhang, J. Power Sources 196 (2011) 4436.
[3] D. Linden, T.B. Reddy, Handbook of Batteries, third ed., 2002, p. 38.46.
[4] B. Horstmann, T. Danner, W.G. Bessler, Energy Environ. Sci. 6 (2013) 1299.
[5] S. Zhuang, K. Huang, C. Huang, H. Huang, S. Liu, M. Fan, J. Power Sources 196 (2011) 4019.
[6] H. Ohkuma, I. Uechi, N. Imanishi, A. Hirano, Y. Takeda, O. Yamamoto, J. Power Sources 223 (2013) 319.
[7] X. Liu, D. Wang, S. Shi, Electrochim. Acta 87 (2013) 865.
[8] S.S. Zhang, D. Foster, J. Read, J. Power Sources 195 (2010) 1235.
[9] Y. Wang, H. Zhou, J. Power Sources 195 (2010) 358.
[10] A.K. Thapa, T. Ishihara, J. Power Sources 196 (2011) 7016.
[11] J. Xiao, J. Hu, D. Wang, D. Hu, W. Xu, G.L. Graff, Z. Nie, J. Liu, J.-G. Zhang, J. Power Sources 196 (2011) 5674.
[12] P. He, Y. Wang, H. Zhou, J. Power Sources 196 (2011) 5611.
[13] P. Kichambare, J. Kumar, S. Rodrigues, B. Kumar, J. Power Sources 196 (2011) 3310.
[14] C. Laoire, S. Mukerjee, E.J. Plichta, M.A. Hendrickson, K.M. Abraham, J. Electrochem. Soc. 158 (2011) A302.
[15] A. Kraytsberg, Y. Ein-Eli, J. Power Sources 195 (2011) 886.
[16] E. Yoo, H. Zhou, ACS Nano 5 (2011) 3020.
[17] S.A. Freunberger, Y. Chen, Z. Peng, J.M. Griffin, L.J. Hardwick, F. Barde, P. Novak, P.G. Bruce, J. Am. Chem. Soc. 133 (2011) 8040.
[18] S.R. Younesi, S. Urbonaite, F. Björefors, K. Edström, J. Power Sources 196 (2011) 9835.
[19] J. Christensen, P. Albertus, R.S. Sanchez-Carrera, T. Lohmann, B. Kozinsky, R. Liedtke, J. Ahmed, A. Kojic, J. Electrochem. Soc. 159 (2012) R1.
[20] Y. Li, K. Huang, Y. Xing, Electrochim. Acta 81 (2012) 20.
[21] V. Nikolova, P. Iliev, K. Petrov, T. Vitanov, E. Zhecheva, R. Stoyanova, I. Valov, D. Stoychev, J. Power Sources 185 (2008) 727.
[22] Y. Gao, C. Wang, W. Pu, Z. Liu, C. Deng, P. Zhang, Z. Mao, Int. J. Hydrogen Energy 37 (2012) 12725.
[23] H. Wang, Y. Yang, Y. Liang, G. Zheng, Y. Li, Y. Cui, H. Dai, Energy Environ. Sci. 5 (2012) 7931.
[24] P.N. Ross, M. Sattler, J. Electrochem. Soc. 135 (1988) 1464.
[25] P.N. Ross, H. Sokol, J. Electrochem. Soc. 131 (1984) 1742.
[26] H. Arai, S. Müller, O. Haas, J. Electrochem. Soc. 147 (2000) 3584.
[27] D. Wittmaier, T. Danner, N. Wagner, K.A. Friedrich, J. Appl. Electrochem. 44 (2013) 73.
[28] S. Visco, E. Nimon, B. Katz, M. Chu, L. Jonghe, Abstract #1156, Honolulu PRiME, 2012, ECS.
[29] T. Zhang, A. Nobuyuki, J. Electrochem. Soc. 155 (2008) A965.
[30] Y. Shimonishi, T. Zhang, N. Imanishi, D. Im, D.J. Lee, A. Hirano, Y. Takeda, O. Yamamoto, N. Sammes, J. Power Sources 196 (2011) 5128.
[31] International Centre for Diffraction Data (ICCD), PDF-2 Release, USA, 2009.
[32] D. Tudela, J. Chem. Educ. 85 (2008) 863.
[33] M. Lopez Teijelo, J.R. Vilche, A.J. Arva, J. Electroanal. Chem. 131 (1982) 331.
[34] M. Lopez Teijelo, J.R. Vilche, A.J. Arva, J. Appl. Electrochem. 18 (1988) 691.
[35] M. Lopez Teijelo, J.R. Vilche, A.J. Arva, J. Electroanal. Chem. 162 (1984) 207.
[36] N. Sasikala, K. Ramya, K.S. Dhathathreyan, Energy Convers. Manage. 77 (2014) 545.
[37] F.H.B. Lima, J.F.R. de Castro, E.A. Ticianelli, J. Power Sources 161 (2006) 806.
[38] Y. Wang, X. Lu, Y. Liu, Y. Deng, Electrochem. Commun. 31 (2013) 108.
[39] J.K. Norskov, J. Rossmeisl, A. Logadottir, L. Lindqvist, J.R. Kitchin, T. Bligaard, H. Jonsson, J. Phys. Chem. B 108 (2004) 17886.
[40] D. Šepa, M. Vojnovíc, A. Damjanovic, Electrochim. Acta 15 (1970) 1355.
[41] Electrochemical Applications 1/97, ZAHNER-elektrik GmbH & Co. KG, http://zahner.de/pdf/ea1997.pdf.